POLITECNICO DI BARI

Dipartimento di Ingegneria Elettrica e dell'Informazione – DEI

CORSO DI LAUREA MAGISTRALE IN INGEGNERIA INFORMATICA

Ultrasound Images for female Breast Cancer: A Digital Image Processing case study

Professor:
Prof. Andrea Guerriero

Students:
Pietro SPALLUTO
Leonardo RUSSO

Anno Accademico 2020-2021

Contents

List of Figures

List of Tables

List of Acronyms

IoU Intersection-over-Union

NLM Non-Local Mean

PDF Probability Density Function

ROI Region of Interest

US Ultrasound

Introduction

Breast cancer is one of the most spread and hard-to-detect kind of cancer among all humankind, especially in early stages: in fact, this is the cause of death for over 10000/ten thousand women all around the globe [5] but the conformation does not exclude men. This cancer can be found by studying the breast tissues in order to understand whether it can be treated as a non-harmful mass or not and, following the specialist consultations, which medical treatment the patient has to be undergone to.

From the medical theory, a formation of clusters of cells could be a potential representation of a tissue anomaly, i.e. a kind of benign or malignant cancerous anomaly [6]. These formations can manifest even in breast tissue lesions, which locating represents the first way to the early diagnosis. Obviously, the sooner it is discovered by the patient or detected via technologies/medical research, the sooner and the more efficient a cure can result.

Nowadays, technology supports medical work in order to be as efficient as possible, applying tools such as the Medical Image Processing. In the matter in question, the most efficient techniques involved into these surveys are, in order, mammograms and ultrasonography. In the first case, the detection is more accurate even in earlier phases. Certainly, it has a documented 90/ninety percent of accuracy, but the remaining 10/ten percent encloses the human error [6], which should be precisely supported by the Digital Image Processing. The second case, which is also the case study of this report, treats images obtained via shooting ultrasound waves inside the body in order to obtain images. This kind of technology shows a broad selection of applications, but in our case, the breast cancer can be detected with a 85/eighty-five percent of accuracy [7].

In this report, our work is to find the best results with the best algorithms of Image Processing provided by the literature, and to compare our results with some of the achieved ones by medical studies. For this purpose, a dataset of images has been taken from a medical science paper provided by Dr. Fahmy, from now on called "Dataset BUSI" (Breast Ultra-Sound Images) [8], which collects over 780/seven hundred and eighty cases of breast medical examinations, subdivided into benign, malignant, or without a presence of a possible mass.

Each image containing a mass (both benign and malignant) has been firstly segmented manually in order to be ingested to the algorithm and/or to the Image Processing machine, and each image is provided with a variable number of "mask", in the order of 1.5 masks for image, which is the result of a manual and accurate

segmentation done by an experienced Medical Doctor.

In this way, a faster and accurate comparison can be achieved by looking at our results, which are a few compared to the large number of material, and the masks. Note that in this paper our work has been delimited to the analysis of a bunch of images, in equal number for benign and malignant cases.

Chapter 1 describes every algorithm and technique that has been applied for this scope, and any other our team found interesting that could fit well for the application.

Chapter 2 states every application considered explanatory, correlated to each pre-classification of the images.

In chapter 3, the conclusive chapter, results are compared in order to see how far our team's application has been accurate. In this way, it is possible to understand strengths and limits of each algorithm.

Chapter 1

Related Works

For obvious reasons, the percentage of accuracy for this scope of application, in ideal cases, should tend to the 100/hundred, but in real cases an average 87/eighty-seven percent, shored up by a clinical and experienced eye, can save many lives diagnosing the nature of the mass as early as possible, as said in the previous chapter. From now on, six algorithms and techniques commonly applied in medical fields will be summarily described. As aim of our project work, they will be compared in following chapter. Please note that other techniques vastly used, such as Standard Distribution and Clustering [5], or Feature Extraction and Texture Segmentation [9] are not treated in this paper in order to not weigh down the lecturer, but they have been treated as potential material for the final goals and for knowledge.

1.1 Segmentation Algorithms

1.1.1 Region Growing

This algorithm is a procedure that groups pixels or subregions into larger regions using some predefined criteria such as ranges of intensity or colour. It starts with a set of *"seed"* points from which it grows regions by appending to each point the neighbouring pixels that satisfy the parameters [10]. The new pixels are added to the set of seed points and the process is repeated. The selection of similarity criteria depends on the problem and on the type of image. The region growing stops when a stopping rule is met. Figure 1.1 shows the first iterations of a region growing algorithm. The main stopping reason is when no more pixels satisfy the criteria for inclusion, but additional criteria such as size, shape or likeness between a candidate pixel and the pixels grown can be set. Let:

- *f(x, y)* denote an input image;
- *S(x, y)* denote a seed array containing 1s at the location of seed points and 0s elsewhere;
- Q denote a predicate to be applied at each pixel.

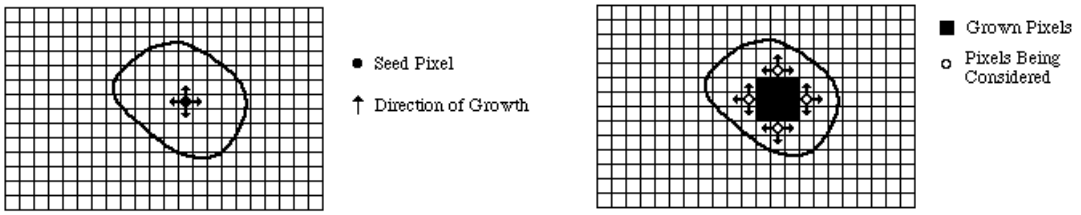

(a) Start of region growing

(b) Region growing after a few iterations

Figure 1.1: Example of region growing [1]

Arrays f and S have the same size.

A simple region growing algorithm is based on 4-connectivity (the pixels are connected to the seed horizontally and vertically) or 8-connectivity (the pixels are connected also diagonally) and follows 4 steps:

1. The seed pixels are compared to their 8-connected neighbours;
2. If any of the neighbouring pixels satisfy the predicate Q that pixel become part of the set S;
3. The comparison is repeated for every new pixel assigned to the set S until a stopping criterion is met;
4. Other regions could be grown using the first unassigned pixel to the previously grown region.

1.1.2 Watershed

In watershed segmentation the 2-D grayscale image is seen as a three-dimensional topological surface being gradually flooded, in which the location is given by the x and y coordinates and the height is the grayscale value of a pixel [11]. In this interpretation three types of points are considered:

1. Points belonging to a regional minimum;
2. Points at which a drop of water would fall with certainty to a single minimum;
3. Points at which water would be equally likely to fall to more than one minimum.

The second category of points identifies a set of points called *catchment basin* or *watershed* of a minimum. The basins are homogeneous in the sense that all the pixels belonging to the same watershed are connected with the basin's region of minimum altitude (graylevel) by a simple path of pixels. The third category identifies the points that constitute the *ridge lines* or watershed lines. The idea behind the algorithm is to imagine the surface being gradually flooded from below with water entering through the local minima. The water starts filling the catchment

basins and, when two catchment basins would merge as a result of a further immersion, a dam is built all the way to the highest surface altitude as shown in Figure 1.2. That dam represents the watershed line. When the water level reaches the highest peak, the process stops.

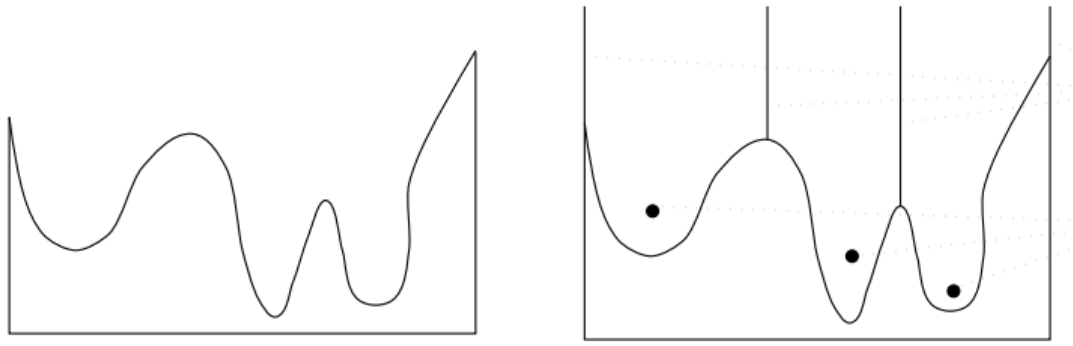

(a) Gray-level profile of image data

(b) Watershed segmentation

Figure 1.2: One-dimensional example of watershed segmentation [2]

Generally speaking, direct application of the watershed segmentation algorithm leads to over segmentation because of noise and other irregularities of the gradient. In this case the result of the algorithm is useless. A solution is to limit the number of allowable regions by incorporating a pre-processing stage to bring additional knowledge to the procedure. The usage of *markers* limits the over segmentation. A marker is a connected component belonging to an image and could be classified into internal or foreground marker, associated with objects of interest and external or background marker, associated with the background. Markers are selected using a set of criteria or via grayscale morphological operation of opening, closing and reconstruction. Once the markers are calculated the image is modified so that it has regional minima in certain location. The method is strongly dependent on the specific nature of the image thus it does not generalize well, and each problem must be treated independently [10].

1.1.3 Mean Shift

This algorithm is based on a gradient-based method to estimate the probability of density. Gradient-based methods first calculate the gradient and then the kernel, a weighting function used in estimation techniques, is shifted by a specific length vector in the direction of a maximum increase of density. The magnitude is the step size which must be chosen appropriately, and this task slows down the convergence. The mean shift solves the problem of gradient methods treating the points in D-dimensional feature space as a probability density function where dense regions correspond to local maxima. Gradient ascent is performed in the feature space on the local density estimation until convergence. At the end of the procedure, stationary points correspond to the modes of the distribution. In this case the step

size is adaptive and depends on the gradient of the density of probability. The gradient is not calculated, instead, a mean shift vector is calculated that points in the same direction as the gradient in gradient-based methods [12].

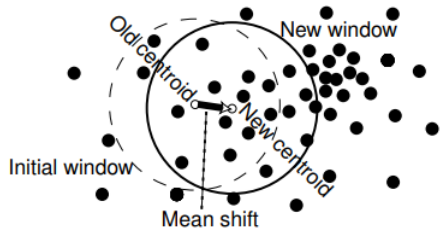

(a) The initial region of interest is randomly positioned over data and its centroid is determined.

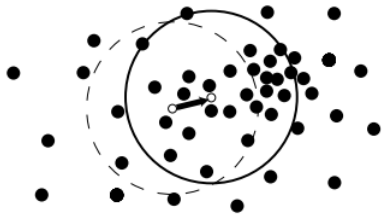

(b) A new mean shift vector is determined and the region is moved accordingly.

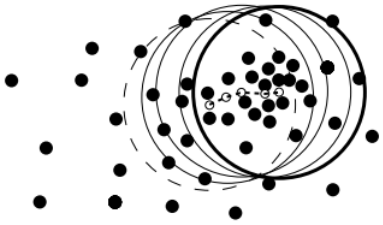

(c) The mean shift vectors are determined in the remaining steps of the procedure until convergence.

Figure 1.3: Principle of the mean shift procedure, the most dense region of data is identified in an iterative process [2]

Mean shift algorithm, in contrast to K-means, does not need assumptions on the number of clusters and the shape of distribution, it only relies on the selection of the kernel size called bandwidth. The mean shift consists of two steps:

1. Construction of probability density in a feature space;

2. Mapping of each point to the maximum of the density which is closest to it

Each data point is shifted to the weighted average of the data set. The mean shift tries to find stationary points of an estimated Probability Density Function (PDF).

During the process of segmentation, the points that are closer than the bandwidth are grouped together and in the end are labeled. When the mean shift procedure is applied to every point in the feature space, the points of convergence aggregate in groups that can be merged. These are the detected modes, and the associated data points define their basins of attraction. Figure 1.3 shows the mean shift procedure until convergence.

1.1.4 K-means

The k-means technique *"is a process of partitioning an N-dimensional population into k sets on the basis of a sample"* [13]. This technique aims to reallocate data points to their closest ones, starting either from a random seed or from K data points that could be provided at the processing, then recomputed as a centroid of their associated data points, calculating a distance metric. Euclidean is the most common distance metric used for this purpose. This calculus for centroids must consider an optimal distance among them as much larger as possible. In Figure 1.4 are illustrated some steps of the algorithm.

(a) Distribution of points.

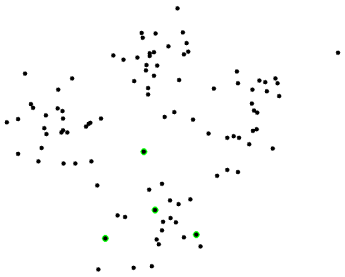

(b) Selection of centroids.

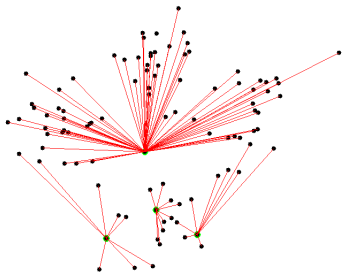

(c) Calculation of distance from other points.

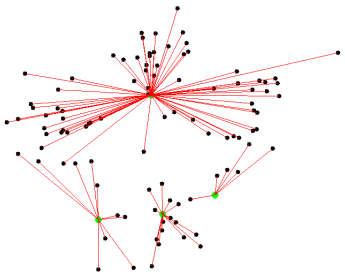

(d) Position of centroids after some iterations.

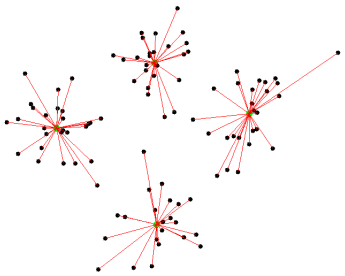

(e) Last iteration.

Figure 1.4: Illustration of k-means algorithm

The steps that a general k-means algorithm covers are the following [13]:

- Define k centroids, one for each cluster. Every centroid should be as far from each other as possible;

- Associate each point belonging to the set of data (in our case, the set of pixels belonging to the image) to its nearest centroid;
- Run a new iteration for calculating centroids, and compare the results with the previous ones;
- Compare the set of data with the new centroids. As result, centroid have been geometrically moved;
- Loop last three points until centroids don't move any more.

1.1.5 Graph Cut

As its name states from Graph theory, Graph Cut, or *minimum cut*, is a segmentation criterion that supposes the image as a set of vertices linked to each other via edges, applying a cut onto them, as seen in Figure 1.5. In other words, the set of pixels and their links can be simplified as a undirected weighted graph $\mathbf{G}$=($\mathbf{V}$,$\mathbf{E}$), from which two disjointed sets can be obtained. This amount can be computed as the total weight of the removed edges [3]. In formula:

$$cut\,(A, B) = \sum_{u \in A, v \in B} w\,(u, v) \tag{1.1}$$

This summation represents the value that minimizes the cut, which brings to understand that a simple graph cut, in some cases, could only isolate some vertices, whether they could be only one or more than one. In this way it is possible to obtain a minimum cut, but at the cost of isolated nodes.

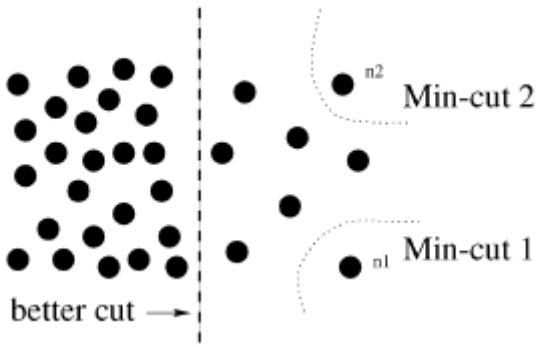

Figure 1.5: Graph cut example [3].

1.1.6 Normalized Cut

Once analyzed the Graph Cut and its possible occurring limitations in Image Processing, a focus on its improvement, the Normalized Cut segmentation, is mandatory.

The focus is moved onto the normalized cut Ncut(A,B), which no more gives out min cut with isolated nodes, as seen in 1.5, but brings out a large percentage of the overall connections among nodes. In formula [3]:

$$Ncut\,(A,B) = \frac{cut\,(A,B)}{assoc\,(A,V)} + \frac{cut\,(A,B)}{assoc\,(B,V)} \tag{1.2}$$

where *assoc(A,V)* represents the total links from A to the graph, and same for *assoc(B,V)*; in other words, they represent the *w(u,v)*. This sum is the starting point for the second part of the algorithm, which consists of a calculus of eigenvalues λ for *"computing optimal partitions"* [3]. Omitting the proof, the eigensystem comes from the following:

$$(\mathbf{D} - \mathbf{W})\,y = \lambda \mathbf{D} y \tag{1.3}$$

In the formula, the understandable fact is that the eigenvalues, and consequent eigensystems, are described by:

- **D**: *N x N* diagonal matrix of $d_{i,j}$ total connections from node i to the other nodes;
- **W**: *N x N* symmetrical matrix with *W(i,j)*=$w_{i,j}$;
- y: a substitute expansion of x=N=|V| dimensional indicator vector which assumes 1 if node i∈A and -1 otherwise.

At this point, from the eigensystem resolution based on the smallest eigenvalue, a bipartition of the graph can be applied with the computing of the second smallest eigenvalue. Note that this procedure is recursive at will by giving the appropriate parameter.

The following images (Figures 1.6a, 1.6b, 1.6c) show how much importance is given to the eigensystem chosen. In fact, the second and the third image show, respectively, the second and the third smallest eigensystems' results.

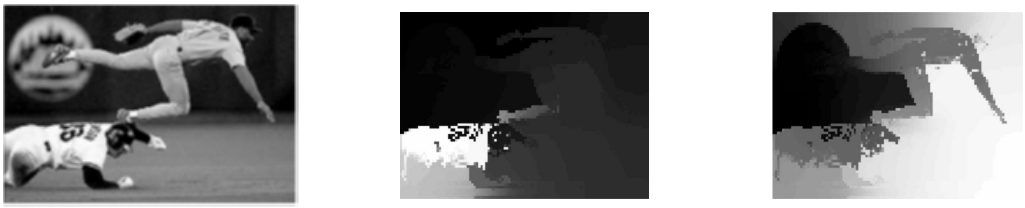

(a) (b) (c)

Figure 1.6: (a) shows the original image. (b) and (c) show the result of the segmentation [3]

1.2 Noise Filters

Ultrasound (US) is a sound wave with a frequency that exceeds 20 kHz. It transports energy and propagates through several means as a pulsating pressure wave.

It is described by a number of wave parameters such as pressure density, propagation direction, and particle displacement.

The usefulness of US imaging is degraded by the presence of signal dependent noise known as speckle. Speckle noise is multiplicative in nature and it is an inherent property of medical US imaging: because of this noise the image resolution and contrast become reduced, which effects the diagnostic value of this imaging modality. So, speckle noise reduction is an essential pre processing step, whenever US imaging is used for medical imaging.

This kind of multiplicative and non-Gaussian noise is more difficult to remove than additive noise because the intensity of the noise varies with the image intensity [14].

1.2.1 Adaptive Filters

The adaptive filters are widely used in US image restoration because they are easy to implement and control. The commonly used adaptive filters are the Lee's filter [15], Frost's filter [16], and Kuan's filter [17] assume that speckle noise is essentially a multiplicative noise. An adaptive filter behaviour changes based on statistical characteristics of the image inside the filter defined by the m x n window S_{xy}. The mean and variance of a random variable are the simplest statistical measures and are closely related to the appearance of an image. The mean gives a measure of average intensity in the region over which the mean is computed, and the variance gives a measure of contrast in that region. The response of the filter at any point *(x, y)* of the image *f(x, y)* is based on four quantities:

- The value of the noisy image at *(x, y)*, denoted with *g(x, y)*;
- The variance of the noise, denoted with ${\sigma_\eta}^2$;
- The local mean of the pixels, denoted with $\mathrm{m_L}$;
- The local variance of the pixels, denoted with ${\sigma_\mathrm{L}}^2$;.

If ${\sigma_\eta}^2$ is zero, the filter returns the value of *g(x, y)* which is equal to *f(x, y)*. If the local variance is high relative to ${\sigma_\eta}^2$ the filter returns a value close to *g(x, y)* because a high variance is associated with edges, and these should be preserved. Finally, if ${\sigma_\eta}^2$ and ${\sigma_\mathrm{L}}^2$ are equal, the filter returns the arithmetic mean value of the pixel in the region S_{xy} because the local area has the same properties of the overall image and the noise is reduced simply by averaging.

The resulting image based on the previous assumption is obtained by using the following expression:

$$\widehat{f}(x,y) = g(x,y) - \frac{\sigma_\eta^2}{\sigma_L^2}\left[g(x,y) - m_L\right] \tag{1.4}$$

The only quantity that needs to be known or estimated is ${\sigma_\eta}^2$ because the other parameters are calculated from the pixels in S_{xy}.

1.2.2 NLM Filters

As soon as an image, supposed in scales of gray for this purpose, is captured, it comes out with noise: this gain to the image could infer into its own manipulation. Filters are used to solve this issue removing noisy measurements, in order to obtain an image as tending to the initial image as possible, but without artifacts.

In mathematical terms, it is possible to write the following model which takes into account the variation at each pixel i:

$$v(i) = u(i) + n(i) \tag{1.5}$$

where:

- *v(i)*: observed value;
- *u(i)*: actual value;
- *n(i)*: noise perturbation.

The NLM algorithm allows to reduce the noise by comparing more pixels with each other via their own weighted average. These weights depend on the similarity between pixels i and j, as per the following [18]:

$$NL\left[v\right](i) = \sum_{j \in I} w(i,j) \cdot v(j) \tag{1.6}$$

It is obvious that the similarity, in the case study, corresponds to the difference between the scales of gray belonging to each pixel. This is called "pixelwise approach" (Figure 1.7a).

Even in this algorithm, the Euclidean distance takes place, although it sustains the order of similarity between the two measures: this means that the algorithm has an intrinsic robustness.

(a) Pixelwise NL-Filter.

(b) Blockwise NL-Filter.

Figure 1.7: Two different approaches to NLM Filters [4].

NLM filter can be applied following another possible approach, which is based not the pixels, but on blocks of pixels [4] (Figure 1.7b): in this way, a series of blocks are restored and compared to each other in order to apply the same logic that flows with the pixelwise approach, but on blocks, and a decreasing operational load is experienced. [4].

Chapter 2

Algorithms and applications

In this chapter some segmentation algorithms will be treated. Before the application of any segmentation algorithm some pre-processing operations are needed to enhance the images and therefore to increase the accuracy of the segmentation process.

The first step is the individuation of a ROI to reduce the size of the image and the computational complexity of the segmentation algorithm.

The next step is the reduction of the speckle noise. In this case a blockwise Non-Local Mean Filter is used.

The last step is the constrast stretching. Ultrasound RGB images were converted into HSV color model and the constrast enhancement was performed only on V channel. The resultant V was subtracted from the initial V and the image was reconverted to RGB [19]. The reason of the conversion is that HSV model performs better because the description of the image in terms of hue, saturation and value do not separate colour into their three value components according to human perception but is more relevant for image analysis [20].

2.1 K-means application

About k-means algorithm, the main parameter is, intuitively, the number of clusters k, which gives a variable-accurate image pre-processing for further applications: so, the number of segments involved is obviously proportional to k. But as k raises, the sharpness of the image is not consequently higher, as seen in Figure 2.4. In fact, at k different values for different images, there could occur that the k-means application could give approximately the starting image, but for smaller k values (not equal to 1 because of the impossibility to distinguish more scales of gray than the medium one), a well-defined image in gray scales can be obtained in order to find our objective.

For our purpose, the main k-means algorithm and the spatial version are applied. Note that the chosen image in Figure 2.1 is the candidate one, on which a ROI will be cut out.

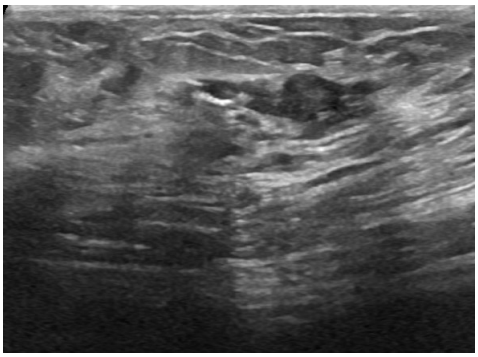

Figure 2.1: Candidate image for k-means application

Furthermore, the choosing of a ROI, depicted in Figure 2.2 is mandatory, so to reduce the processing time and to let the algorithm work on the sole objective. The resultant one is ingested to the Speckle Reduction algorithm and, after that, to the Contrast Stretching one so to lighten the designated computational burden of the k-means.

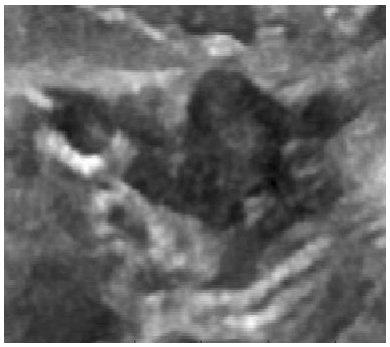

Figure 2.2: ROI extracted from Figure 2.1

The results, as per the passages for a brief interpretation of these phases, are reported in Figure 2.3.

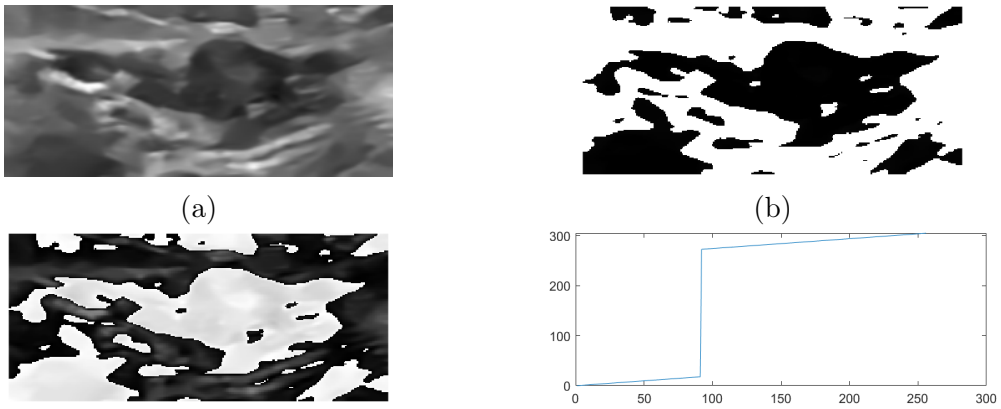

(a) (b) (c) (d)

Figure 2.3: (a) image without noise using Speckle Removal; (b) Contrast Stretching applied to the V channel of the figure; (c) output of the RGB image with contrast enhancement; (d) values and thresholds for the grayscale after constrast stretching.

After these, the image has to be given to the k-means one, which compares the centroids in function of k value, and gives as output an average value of these k clusters. But for achieving our final goal it is mandatory to run the k-means spatial version, which guarantees an optimization process by considering the geometric centroids (in major cases, Euclidean). Figure 2.4 states the differences in these cases study, of a little variation of k, separated for class of belonging. The application for high values of k is omitted.

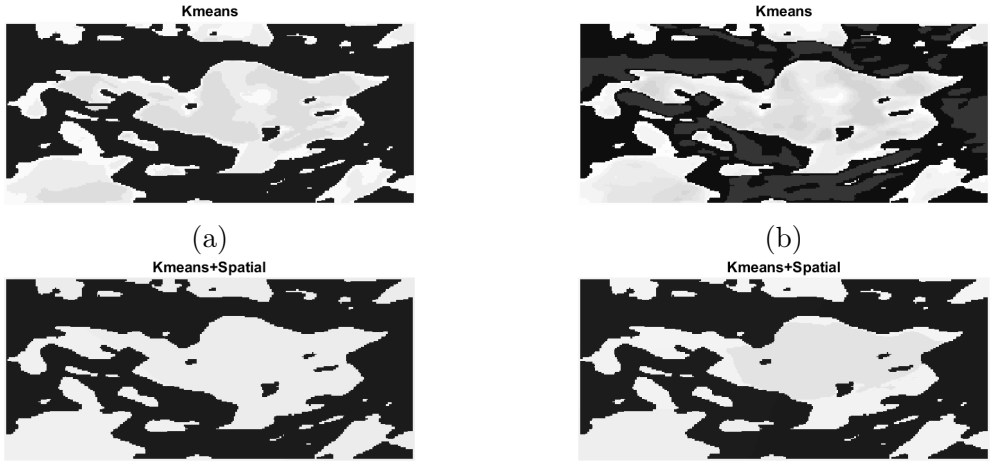

(a) (b) (c) (d)

Figure 2.4: Two different applications of k-means at k equal to 4/four (figures (a) and (c)) and 8/eight (figures (b) and (d)). Figures (a) and (b) can be compared for application of simple k-means algorithm, while (c) and (d) for spatial one.

2.2 Region growing application

The region Growing application consists of a seed choosing, which is the base for extracting the feature needed for every application. Using the same starting image of the previous paragraph, Figure 2.3a, a Contrast Stretching pre-processing is applied and its output converted into grayscales format in order to be run to the region growing segmentation process.

The set of seeds is chosen starting from the output of the preprocessing, and Figure 2.5 shows all these passages. With this one, the algorithm starts with the similarity criteria [10] that are suitable for our problem.

(a)

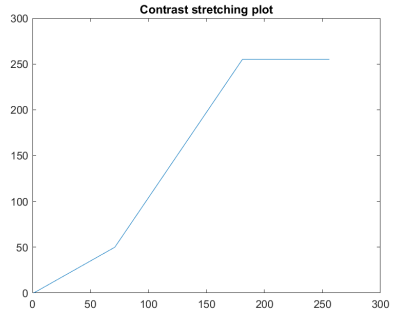

(b)

(c)

Figure 2.5: Results of (a) pre-processing with different values and thresholds, as stated in the (b) plot. (c) Region Growing application.

2.3 Mean shift application

Here, a flat kernel is being used and his size, the bandwidth, is the only parameter in the mean shift. It is important to choose the right value for the bandwidth because the output depends on the kernel size. A small kernel increases the computational complexity but gives better results than a larger kernel. Using a small kernel more clusters are created.

In Figure 2.6 the unprocessed image of a malignant breast cancer is shown. This image cannot be easily processed because of its own size.

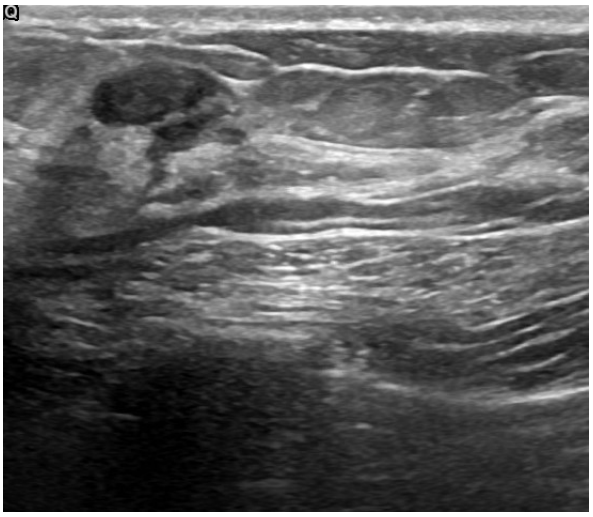

Figure 2.6: Selected image

Once selected a ROI, Figure 2.7, the contrast of the smaller image is enanched before the actual segmentation.

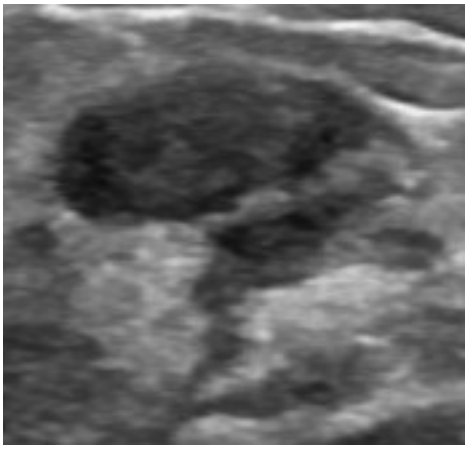

Figure 2.7: ROI of the image

The pre-processing is shown in Figure 2.8.

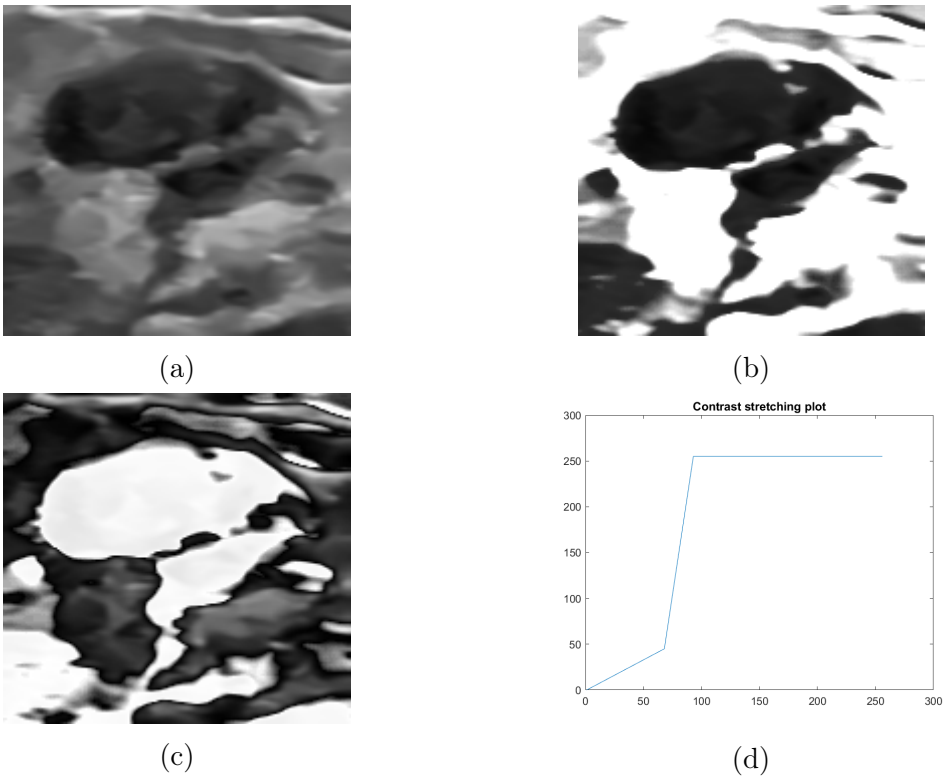

Figure 2.8: (a) shows the denoised image using a blockwise NLM filter. (b) represents the contrast stretching applied on the V channel. (c) shows the RGB image after the contrast enanchement. (d) is the plot of the grayscale values after the stretching.

The final step is the segmentation. In Figure 2.9 three different values of the bandwidth are used with very similar results. In this case the computational complexity increases but the actual mask that will be used to discuss the results is almost the same.

(a) bandwidth = 0.2, cluster = 3

(b) bandwidth = 0.5, cluster = 2

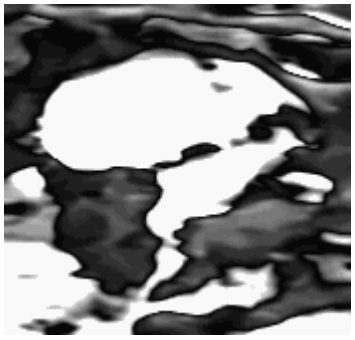

(c) bandwidth = 0.05, cluster = 21

Figure 2.9: Reducing the size of the kernel the numer of clusters and the computational complexity increase. The masks that will be obtained from these three segmentations are similar.

2.4 Watershed application

Marker controlled watershed is useful to avoid an oversegmentation as a result of the algorithm. A series of morphological techniques are used to clean the image and create a flat maxima inside the foreground objects. These techniques are based on two basic morphological operators.

The erosion is one fundamental operation in morphological processing and it is defined as:

$$A \ominus B = \{z | B_z \subseteq A\} \tag{2.1}$$

where:

- A: is the image to be eroded;
- B: is the structuring element;
- z: is the result of the erosion.

In words, the erosion of$A$ by B is the set of all points z such that B, translated by z, is contained in A. At the end of the process the image is thinner and components smaller than the structuring element are removed.

Dilation is the dual operation of erosion and is defined as:

$$A \oplus B = \left\{ z | (\widehat{B})_z \cap A \neq \emptyset \right\} \tag{2.2}$$

where:

- A: is the image to be dilated;
- $\hat{B}$: is the reflection of B about its origin;
- z: is the result of the dilation.

Similar to the erosion, in the dilation $\hat{B}$ is shifted by z. The dilation is the set of all displacements such that $\hat{B}$ and A overlap by at leas one element. Unlike erosion, the result of a dilation is a thicker image [10].

The first operation applied is the opening-closing by reconstruction. Opening-closing consists of an opening, that is an erosion followed by a dilation, followed by a closing, namely a dilation followed by an erosion. The opening it's denoted as:

$$A \circ B = (A \ominus B) \oplus B \tag{2.3}$$

The general effect of opening is to remove small, isolated objects from the foreground of an image, placing them in the background. It tends to smooth the contour of a binary object and breaks narrow joining regions in an object. We instead denote closing as:

$$A \bullet B = (A \oplus B) \ominus B \tag{2.4}$$

Closing tends to remove small holes in the foreground, changing small regions of background into foreground. It tends to join narrow isthmuses between objects.

The morphological reconstruction restores exactly the shapes of an object after the opening-closing operation. However, the accuracy of the restoration is higly dependent of the similarity of the shapes of the object that remains after the process

The result of opening-closing by reconstruction does not affect the shape of objects and still removes small black regions.

After the preprocessing steps shown in Figure 2.11, the morphological operation of opening-closing by reconstruction is applied to the enhanced image using two different structuring elements: a disk with a five pixels radius and a disk with a twenty pixels radius.

Due to the dimensions of the ROI (590x419 pixels), a bigger structuring element gives better results, as can be seen in Figure 2.12. The black region present inside the tumor in Figure 2.13b is brighter than the same region in Figure 2.13a, this is enough to have good results during the segmentation process.

After finding the markers, using the regional maxima, and computing the watershed ridge lines thresholding the images obtained with the opening-closing by reconstruction operation, the watershed algorithm is executed.

Figure 2.10: Original image

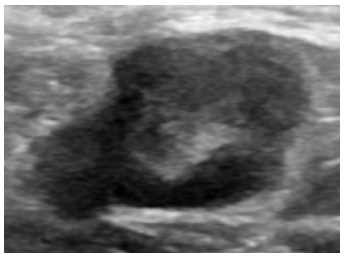

(a) ROI of the original image

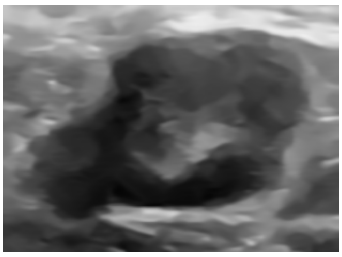

(b) Image after the speckle removal using NLM filter

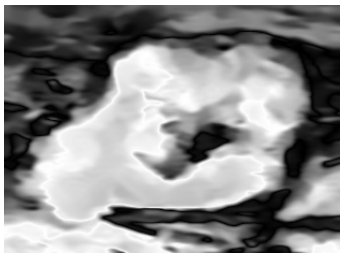

(c) Contrast enhancement

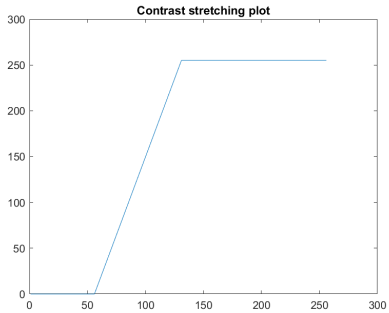

(d) Contrast enhancement plot

Figure 2.11: Preprocessing steps applied to Figure 2.10

In Figure 2.13 there is the comparison between the results of the morphological operations using the two different structuring elements.

(a) Opening-closing by reconstruction using a five pixels radius disk as structuring element. More regional maxima are present.

(b) Opening-closing by reconstruction using a twenty pixels radius disk as structuring element.

Figure 2.12: Results of opening-closing by reconstruction.

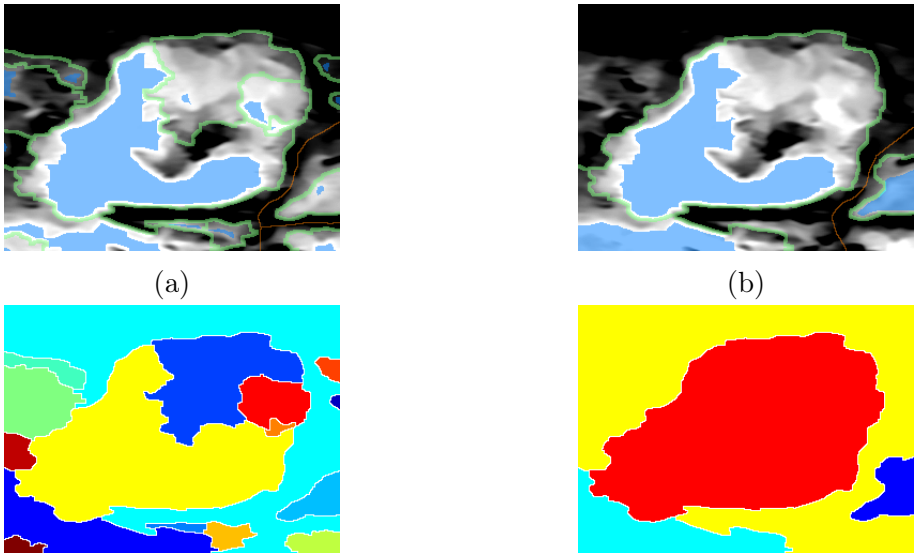

(a)

(b)

(c)

(d)

Figure 2.13: Markers (blue), boundaries (green) and ridge lines (orange). In (a) there are more foreground markers due to the usage of a five pixels radius disk, this caused an over-segmentation. Furthermore the black region inside the tumor is considered as a separated one. A proper morphological operation solves this problem. Images (c) and (d) represents the different regions of the image created using respectively a five pixels radius disk and a twenty pixels radius disk as structuring element.

Conclusions

In this chapter, the application of the algorithms give us the "masks", i.e. the results of the segmentation, which denote black and white images for comparison of the manually segmented ones by Medical Doctors [8].

For this purpose, two additional algorithms, used for comparing similarity between the masks, are implemented. The evaulation metrics obtained are the Dice coefficient and the Intersection-over-Union (IoU). Given two sets of data, A and B, that in our case represent the mask obtained from one of the segmentation algorithms treated previously and the ground truth mask the two metrics are defined as:

- **IoU:**

$$IoU = \frac{|A \cap B|}{|A \cup B|} \tag{2.5}$$

  IoU, also known as Jaccard index, is the most commonly used metric for comparing the similarity between two arbitrary shapes. IoU encodes the shape properties of the objects under comparison, e.g. the widths, heights and locations of two bounding boxes, into the region property and then calculates a normalized measure that focuses on their areas (or volumes). This property makes IoU invariant to the scale of the problem under consideration. Due to this appealing property, all performance measures used t evaluate for segmentation, object detection, and tracking rely on this metric [21].

- **Dice similariry coefficient:**

$$D = \frac{2\,|A \cap B|}{|A| + |B|} \tag{2.6}$$

  This second evaluation metric is very similar to the IoU, in fact they arre correlated, but Dice coefficient better reflects size and localization agreement for object segmentation [22].

In order to find whether our application could give results as nearest as possible to the manually segmented ones provided by the Dataset the same ROI is applied to the resulting mask and to the ground truth mask.

In the following, some masks are obtained segmenting the images and are put next to each other for comparison. Note that each image has been ingested to an image processing algorithm, already treated in Chapter 2, and some parts of the

tumor are hidden in the original US image but not in the ground truth mask. Due to this the output masks of the segmentation could never be perfectly accurate.

K-means results

In this application, the k-means, as stated in the previous chapter, gives worse results with gradually increasing of number of clusters. Figure 3.1 shows a rapid comparison between the four images, where a k=4 and a k=8 has been chosen. For further details about metrics, please read Table 1.

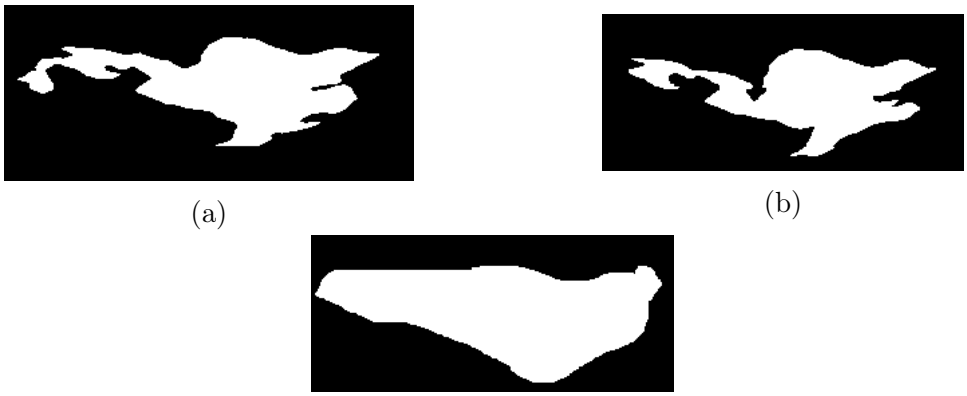

(a) (b)

(c)

Figure 3.1: a comparison between variations of cluster number: (a) k=8, (b) k=4 and (c) mask obtained from same ROI

Table 2.1: Comparison between masks' ROIs from k-means algorithm

Image compared to Figure 3.1c	Clusters	IoU	Dice
Figure 3.1b	8	55.58%	71.45%
Figure 3.1a	4	65.52%	79.17%

From Table 2.1, a glaring result on low value of clusters can be no-ticed: as said in Chapter 2, the more clusters are involved, the less segmentation is experienced, and it can be read from the re-duced indexes at major values of k. Note that the image taken into consideration has been chosen randomly, and then used also in k-means application in Chapter 2.1, among the malignant ones and pre-processed with speckle removal and contrast stretching, in order. It can be found as Malignant (141) in Da-taset BUSI.

Region growing results

As literature states, an application of Region Growing algorithm starts from a set of pixels from which the segmentation has to be done, comparing 4-way or 8-way. In our approach, we have cho-sen to apply a simple 5% threshold to the segmentation and to give the opportunity to the user to choose the best starting seed. This lets us understand that values of the Contrast Stretching must be placed wisely, so to correctly manipulate the resulting mask. Results can be read in 2.2 and in Figure 3.2.

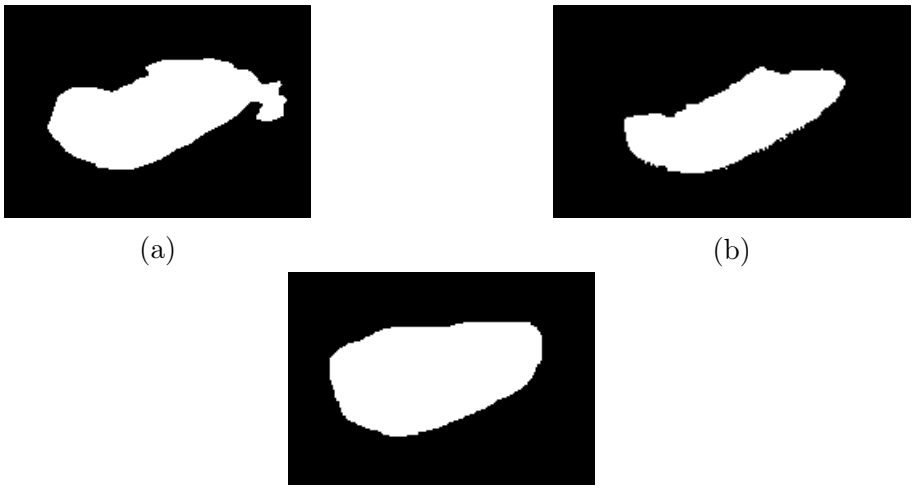

(a) (b)

(c)

Figure 3.2: (a) Mask obtained from first segmentation, (b) Mask obtained from second segmentation. (c) Actual handmade segmentation, i.e. ground truth mask.

Note that values of thresholds are not so different, as highlighted in the plots from Figure 3.2a and 3.3b, but that's enough to say that this kind of segmentation for medical purposes is is strongly affected by a well pre-processed image via constrast stretching.

Table 2.2: Comparison between masks' ROIs from Region Growing algorithm with a constant 5% offset.

Image compared to Figure 3.2c	IoU	Dice
Figure 3.2a	77.06%	87.04%
Figure 3.3b	69.43%	53.17%

Mean shift results

As previously said, the three masks obtained using the mean shift segmentation are almost the same. In this case, a proper contrast stretching is probably more important than the selection of the bandwidth. An image like the one segmented using this algorithm has small pieces that can only be highlighted with a contrast enhanchement process. In the Figure 3.3 is shown the comparison between the ground truth mask and only one of the three masks obtained.

(a) (b)

Figure 3.3: (a) Mask obtained from the mean shift segmentation using a bandwidth of 0.2 and (b) ground truth mask.

In the Table 2.4 are listed the values of the IoU and the Dice coefficient. Even if the value of the bandiwidth in the first row is ten time bigger than the value of the bandiwidth in the last row the indexes are almost identical.

Table 2.3: Comparison between the metrics using three masks.

Means shift bandwidth	IoU	Dice
0.5	66.47%	79.86%
0.2	64.76%	78.61%
0.05	64.30%	78.27%

Watershed results

The watershed needs more pre-processing compared to the previous algorithms but gives also better results. This is the only algorithm, among the four used algorithms, that can include some of the hidden or darker regions in the segmentation, that are present in the ground truth mask but usually excluded because the image is not clean enough.

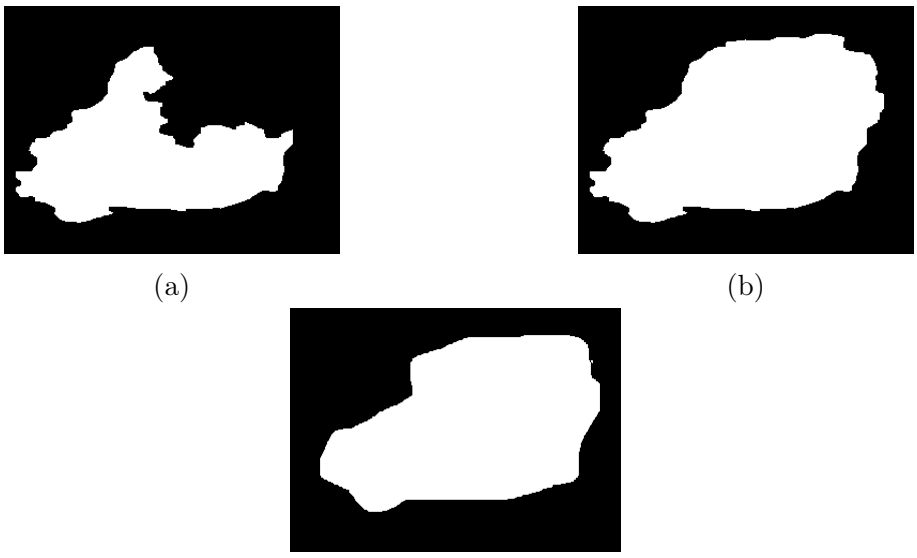

(a) (b)

(c)

Figure 3.4: (a) Mask obtained using a disk of 5 pixels, (b) mask obtained using a disk of 20 pixels and (c) ground truth mask.

The difference between the two obtained masks is clearly visible. A small structuring element can't clean the image, especially a big image or an image with big darker regions, if used in the opening-closing by reconstruction because it is too precise. The image used as example has a big dark region in its center, but an opening-closing by reconstruction with a proper structuring element, a 20 pixel radius disk in this case, can decrease the difference between the intensity level of this region and the intensity level of the surrounding brighter region leading to much better results.

Table 2.4: Comparison between two different segmentations.

Disk radius	IoU	Dice
5	59.28%	74.43%
20	92.17%	95.93%

Bibliography

[1] Xiaoli Zhang, Xiongfei Li, and Yuncong Feng. A medical image segmentation algorithm based on bi-directional region growing. *Optik*, 126(20):2398–2404, 2015.

[2] Milan Sonka, Vaclav Hlavac, and Roger Boyle. *Image Processing, Analysis and Machine Vision*. Cengage Learning, 2013.

[3] Jianbo Shi and J. Malik. Normalized cuts and image segmentation. *IEEE Transactions on Pattern Analysis and Machine Intelligence*, 22(8):888–905, 2000.

[4] Pierrick Coupe, Pierre Hellier, Charles Kervrann, and Christian Barillot. Non-local means-based speckle filtering for ultrasound images. *IEEE Transactions on Image Processing*, 18(10):2221–2229, 2009.

[5] Ranjeet Singh Tomar, Tripty Singh, Sulochana Wadhwani, and Sarita Singh Bhadoria. Analysis of breast cancer using image processing techniques. In *2009 Third UKSim European Symposium on Computer Modeling and Simulation*, pages 251–256, 2009.

[6] Chaitanya Varma and Omkar Sawant. An alternative approach to detect breast cancer using digital image processing techniques. In *2018 International Conference on Communication and Signal Processing (ICCSP)*, pages 0134–0137, 2018.

[7] Uswatun Khasana, Riyanto Sigit, and Heny Yuniarti. Segmentation of breast using ultrasound image for detection breast cancer. In *2020 International Electronics Symposium (IES)*, pages 584–587, 2020.

[8] Walid Al-Dhabyani, Mohammed Gomaa, Hussien Khaled, and Aly Fahmy. Dataset of breast ultrasound images. *Data in Brief*, 28:104863, 2020.

[9] R. Guzmán-Cabrera, J. R. Guzmán-Sepúlveda, M. Torres-Cisneros, D. A. May-Arrioja, J. Ruiz-Pinales, O. G. Ibarra-Manzano, G. Aviña-Cervantes, and A. González Parada. Digital Image Processing Technique for Breast Cancer Detection. *International Journal of Thermophysics*, 34(8-9):1519–1531, September 2013.

[10] Woods Richards Gonzalez Rafael. *Digital Image Processing*. Pearson, 2008.

[11] Breckon Toby Solomon Chris. *Foundamentals of Digital Image Processing.* Wiley-Blackwell, 2011.

[12] Damir Demirović. An Implementation of the Mean Shift Algorithm. *Image Processing On Line*, 9:251–268, 2019. https://doi.org/10.5201/ipol.2019.255.

[13] Vinod Kumar Dehariya, Shailendra Kumar Shrivastava, and R. C. Jain. Clustering of image data set using k-means and fuzzy k-means algorithms. In *Proceedings of the 2010 International Conference on Computational Intelligence and Communication Networks*, CICN '10, page 386–391, USA, 2010. IEEE Computer Society.

[14] P.S. Hiremath, Prema T. Akkasaligar, and Sharan Badiger. Speckle noise reduction in medical ultrasound images. In Gunti Gunarathne, editor, *Advancements and Breakthroughs in Ultrasound Imaging*, chapter 8. IntechOpen, Rijeka, 2013.

[15] Jong-Sen Lee. Digital image enhancement and noise filtering by use of local statistics. *IEEE Transactions on Pattern Analysis and Machine Intelligence*, PAMI-2(2):165–168, 1980.

[16] Darwin T. Kuan, Alexander A. Sawchuk, Timothy C. Strand, and Pierre Chavel. Adaptive noise smoothing filter for images with signal-dependent noise. *IEEE Transactions on Pattern Analysis and Machine Intelligence*, PAMI-7(2):165–177, 1985.

[17] A. Lopes, R. Touzi, and E. Nezry. Adaptive speckle filters and scene heterogeneity. *IEEE Transactions on Geoscience and Remote Sensing*, 28(6):992–1000, 1990.

[18] A. Buades, B. Coll, and J.-M. Morel. A non-local algorithm for image denoising. In *2005 IEEE Computer Society Conference on Computer Vision and Pattern Recognition (CVPR'05)*, volume 2, pages 60–65 vol. 2, 2005.

[19] Misbah Hoque, T M Shahriar Sazzad, A.K.M. Farabi, Ismail Hosen, and Mursheda Somi. An automated approach to detect breast cancer tissue using ultrasound images. pages 1–4, 05 2019.

[20] S. Sazzad, Sabrin Islam, Mohammad Mahbubur Rahman Khan Mamun, and Md Hasan. Establishment of an efficient color model from existing models for better gamma encoding in image processing. *International Journal of Image Processing*, 7:90 – 100, 02 2013.

[21] Hamid Rezatofighi, Nathan Tsoi, JunYoung Gwak, Amir Sadeghian, Ian Reid, and Silvio Savarese. Generalized intersection over union: A metric and a loss for bounding box regression. In *2019 IEEE/CVF Conference on Computer Vision and Pattern Recognition (CVPR)*, pages 658–666, 2019.

[22] Tom Eelbode, Jeroen Bertels, Maxim Berman, Dirk Vandermeulen, Frederik Maes, Raf Bisschops, and Matthew B. Blaschko. Optimization for medical image segmentation: Theory and practice when evaluating with dice score or jaccard index. *IEEE Transactions on Medical Imaging*, 39(11):3679–3690, 2020.